*Supporting Information for:*

# TEMPLATE-FREE SYNTHESIS OF PERIODIC THREE-DIMENSIONAL PBSE NANOSTRUCTURES VIA PHOTOELECTRODEPOSITION

AZHAR I. CARIM[†,⊥], KATHRYN R. HAMANN[†,⊥], NICOLAS A. BATARA[‡], JONATHAN R. THOMPSON[‡], HARRY A. ATWATER[‡,§] AND NATHAN S. LEWIS[†,§,ǁ,*]

[†]Division of Chemistry and Chemical Engineering

[‡]Division of Engineering and Applied Sciences

[§]Kavli Nanoscience Institute

[ǁ]Beckman Institute

California Institute of Technology

Pasadena, CA 91125

[⊥]These authors contributed equally (AIC and KRH)

*Corresponding Author: nslewis@caltech.edu

## S1. Contents

This document contains a description of the experimental and modeling/simulation methods utilized in this work (Sections S2 and S3), chronoamperometry data (Sections S4), additional scanning-electron micrographs and associated two-dimensional Fourier transform data (Section S5), additional computer simulation data (Section S6), additional grazing-incidence X-ray diffraction data (Section S7), and a list of associated references (Section S8).

## S2. Experimental Methods

*Materials and Chemicals* $(CH_3)_2CO$ (ACS Grade, BDH), $H_2SO_4$ (ACS Reagent, J. T. Baker), buffered HF improved etchant (Transene), In (99.999 %, Alfa Aesar), Ga (99.999 %, Alfa Aesar), $SeO_2$ (99.999 %, Acros Organics), and $Pb(ClO_4)_2 \cdot 3H_2O$ (99%, Acros Organics) were used as received. $H_2O$ with a resistivity ≥ 18.2 MΩ cm (Barnstead Nanopure System) was used throughout. Au-coated $n^+$-Si(100) (< 0.005 Ω cm, As-doped, 525 ± 25 μm, single-side polished, Addison Engineering) was used as a substrate for deposition. Flash-Dry Ag Paint (SPI Supplies), EP21ARHTND Epoxy (MasterBond) and nitrocellulose-based nail polish were used to assemble the working electrodes.

*Substrate Preparation* $n^+$-Si wafers were etched with buffered HF for 30 s, rinsed with $H_2O$, dried under a stream of $N_2$(g), and then immediately transferred to an electron-beam metal evaporator with a base pressure < $10^{-5}$ torr. Using an accelerating voltage of 10 kV, a 10 nm Ti adhesion layer was deposited on the polished side of the wafer using a 50 mA deposition current and then a 50 nm Pt capping layer was then deposited atop using a 150 mA current. The wafers were then transferred to a RF sputterer in which 100 nm of Au was deposited on top of the Pt using a RF power of 80 W. The Au-topped Si sections were then cut into square 0.50 cm by 0.50 cm sections for use as deposition substrates.

*Electrode Preparation* One end of a Sn-coated Cu wire (22 AWG) was bent to form a small, flat coil and the wire was then threaded through glass tubing (6 mm O. D.) such that the coil was just outside the tubing. Epoxy was applied to seal the end of the tube from which the coil protruded. A eutectic mixture of Ga and In was scratched into the unpolished back surfaces of the Au-topped Si sections with a carbide-tipped scribe. The wire coil was then contacted to the unpolished surface and affixed with Ag paint. Nail polish was applied to insulate the unpolished face, the wire-coil

contact, and the exposed wire between the coil and epoxy seal. Immediately before deposition, the surface of each electrode was briefly cleaned using a stream of $N_2$(g).

*Electrode Illumination* Illumination for the photoelectrochemical depositions was provided by narrowband diode (LED) sources (Thorlabs) with respective intensity-weighted average wavelength, $\lambda_{avg}$, values and spectral bandwidths (FWHM) of 528 nm and 32 nm (SOLIS-525C), 626 nm and 17 nm (SOLIS-623C), and 859 nm and 39 nm (SOLIS-850C). The output of each diode source was collected, collimated, and condensed using a bi-convex lens (Ø50.8 mm, f = 60 mm) followed by two aspheric condenser lenses (Ø25.4 mm, f = 16 mm; Ø30 mm, f = 26 mm). For experiments using polarized illumination, a dichroic film polarizer (Thorlabs LPVISE200-A or LPNIRE200-B) was inserted between the aspheric lenses to control the polarization. A 1500 grit ground-glass (N-BK7) diffuser was placed immediately in front of the photoelectrochemical cell to ensure spatial homogeneity of the illumination.

The light intensity incident on the electrode was measured by placing a calibrated Si photodiode (Thorlabs FDS100) instead of an electrode assembly in the photoelectrochemical cell with electrolyte, and the steady-state current response of that Si photodiode was measured. Depositions utilizing the diodes with $\lambda_{avg}$ = 528 nm and 626 nm were performed with a light intensity of 0.500 W $cm^{-2}$ unless otherwise indicated. Depositions utilizing the diode with $\lambda_{avg}$ = 859 nm were performed with a light intensity of 1.500 W $cm^{-2}$.

*Photoelectrochemical Deposition* Photoelectrochemical deposition was performed using a Bio-Logic SP-200 potentiostat. Deposition was performed in a single-compartment glass cell with a quartz window. A three-electrode configuration was utilized with a graphite-rod counter electrode (99.999 %, Sigma-Aldrich) and a Ag/AgCl reference electrode (3.00 M KCl, Bioanalytical Systems). Films were deposited from an aqueous solution of 0.0100 M $SeO_2$, 0.0050

M $Pb(ClO_4)_2$, and 0.100 M $HClO_4$. Deposition was effected by biasing the Au-coated electrode, illuminated as detailed under the above subheading (*Electrode Illumination*), potentiostatically at 0.00 V vs. Ag/AgCl for 10.00 min at room temperature unless otherwise indicated. Deposition resulted in the addition of material in the out-of-plane direction (normal to the face of the electrode). After deposition, the electrode was immediately removed from the cell, rinsed with $H_2O$, and then dried under a stream of $N_2$(g). The Au-coated substrate with top-facing Se-Pb film was mechanically separated from the rest of the electrode assembly. The nitrocellulose-based insulation and the majority of the Ag paint and In-Ga eutectic were then removed mechanically.

*Electrochemical Post-Processing* Electrodes supporting a photoelectrodeposited film were removed from the cell, rinsed with $H_2O$, and then dried under a stream of $N_2$(g). Electrodes were then transferred to a single-compartment glass cell. A three-electrode configuration was utilized with a graphite-rod counter electrode and a saturated calomel reference electrode (SCE, CH Instruments). The electrode was biased potentiostatically at -0.35 V vs. SCE for 5.00 min at room temperature, to effect the reductive elimination of Se from the films and thereby produce stoichiometric PbSe.

*Microscopy* Scanning-electron micrographs (SEMs) were obtained with a FEI Nova NanoSEM 450 at an accelerating voltage of 5.00 kV with a working distance of 5 mm and an in-lens secondary electron detector. Micrographs obtained for quantitative analysis were acquired with a resolution of 172 pixels $\mu m^{-1}$ over ~ 120 $\mu m^2$ areas. Micrographs that were used to produce display figures were acquired with a resolution of 344 pixels $\mu m^{-1}$ over ~ 2 $\mu m^2$ areas.

*Energy-Dispersive X-ray Spectroscopy* Energy dispersive X-ray (EDX) spectroscopy was performed in the SEM using an accelerating voltage of 15.00 kV with a working distance of 5 mm. An Oxford Instruments X-Max Si drift detector was utilized. Spectra were collected in the range

of 0 to 10 keV and quantitative film compositions were derived from these spectra using the "INCA" software package (Oxford Instruments).

*X-ray Diffraction* Grazing incidence X-ray diffraction (GIXRD) was performed using a Bruker D8 Discover diffractometer with a Cu Kα source and a 2-dimensional Vantec detector. The X-rays were directed at a grazing angle $\omega = 0.3\ ^\circ$ above the plane of the sample surface and the detector was swept throughout the entire $2\theta$ range.

## S3. Modeling and Simulation Methods

*Simulation of Film Morphology* The growths of the photoelectrochemically deposited films were simulated with an iterative growth model wherein electromagnetic simulations were first used to calculate the local photocarrier-generation rates at the film surface. Then, mass addition was simulated via a Monte Carlo method wherein the local photocarrier-generation rate weighted the local rate of mass addition along the film surface.

Growth simulations began with a bare, semi-infinite planar substrate. In the first step, the light-absorption profile under a linearly polarized, plane-wave illumination source was calculated using full-wave finite-difference time-domain (FDTD) simulations with periodic boundary conditions along the substrate interface. In the second step, a Monte Carlo simulation was performed in which an amount of mass, equaling that of a 15 nm planar layer covering the simulation area, was added to the upper surface of the structure with a probability *F*:

$$F(G) = \left[1 + G(\mathrm{n}_0\tau_p + \mathrm{p}_0\tau_n) + G^2\frac{\tau_p\tau_n}{\mathrm{n}_i^2}\right]\prod_{i=1}^{3}\frac{x_i}{r_i} \quad \textbf{(Equation 1)}$$

where *G* is the spatially dependent photocarrier-generation rate at the deposit/solution interface, $n_i$ is the intrinsic carrier concentration, $n_0$ is the electron concentration, $p_0$ is the hole concentration, $\tau_n$ is the electron lifetime, $\tau_p$ is the hole lifetime, $x_i$ is the fraction of $i^{th}$ nearest neighbors occupied in the cubic lattice, and $r_i$ is the distance to the $i^{th}$ nearest neighbor. The multiplicative sum in the definition of this probability (Equation 1) serves to reduce the surface roughness of the film so as to mimic the experimentally observed surface roughness.

After the initial Monte Carlo simulation, the absorbance of the new, structured film was then calculated in the same manner as for the initial planar film, and an additional Monte Carlo simulation of mass addition was performed. This process of absorbance calculation and mass

addition was repeated for a total of 18 iterations.

*General Parameters* Se–Pb films were assumed to be undoped (i.e. $n_0 = p_0 = n_i$), a value of $n_I = 10^{10}$ cm$^{-3}$ was used for the intrinsic carrier concentration, and a value of 1 μs was used for both the electron and hole lifetimes.[1-4] A value of n = 1.33 was used as the refractive index of the electrolyte, regardless of wavelength.[5] Simulations of the film morphology utilized the intensity-weighted average wavelengths, $\lambda_{avg}$, of the experimental sources described in Section S2. The electric field vector of the illumination was oriented parallel to the substrate. A two-dimensional square mesh with a lattice constant of 10 nm was used for the simulations. All FDTD simulations were performed using the "FDTD Solutions" software package (Lumerical).

## S4. Chronoamperometry Data

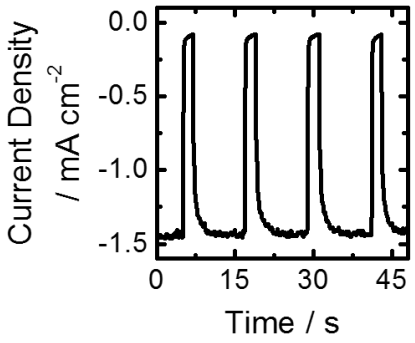


**Figure S1.** Chronoamperometric response under chopped $\lambda_{avg}$ = 626 nm illumination for an electrode supporting a photoelectrodeposited Se-Pb film potentiostatically biased at 0.00 V vs. Ag/AgCl (3.00 M KCl) in a solution containing 0.0100 M $SeO_2$, 0.0050 M $Pb(ClO_4)_2$, and 0.010 M $HClO_4$.

## S5. Additional Scanning-Electron Micrographs and Two-Dimensional Fourier Transform Data

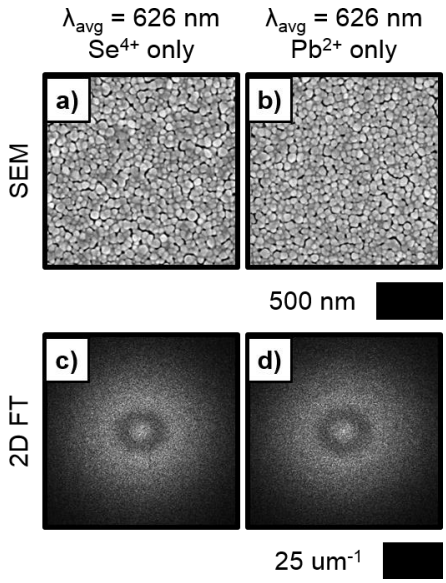


**Figure S2.** SEMs representative of photoelectrodeposits generated using vertically polarized $\lambda_{avg}$ = 626 nm illumination and a solution of (a) 0.0100 M $SeO_2$ and 0.100 M $HClO_4$ and (b) 0.0050 M $Pb(ClO_4)_2$ and 0.100 M $HClO_4$. (c) and (d) 2D FTs generated from SEM data of the deposits depicted in (a) and (b) respectively.

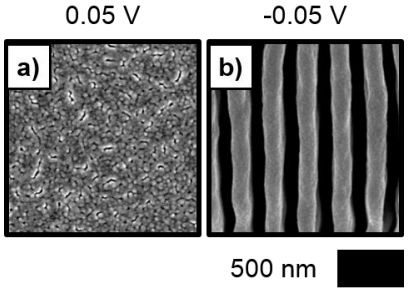


**Figure S3.** (a) and (b) SEMs representative of photoelectrodeposits generated using vertically polarized $\lambda_{avg}$ = 626 nm illumination using the indicated potentiostatic bias relative to Ag/AgCl (3.00 M KCl).

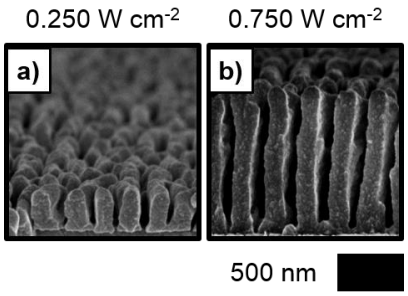


**Figure S4.** (a) and (b) SEMs representative of photoelectrodeposits generated using vertically polarized $\lambda_{avg}$ = 626 nm illumination with the indicated intensity, cleaved along the horizontal axis and acquired in cross-section.

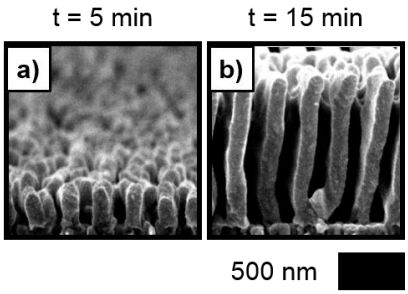


**Figure S5.** (a) and (b) SEMs representative of photoelectrodeposits generated using vertically polarized $\lambda_{avg}$ = 626 nm illumination and the indicated deposition time, cleaved along the horizontal axis and acquired in cross-section.

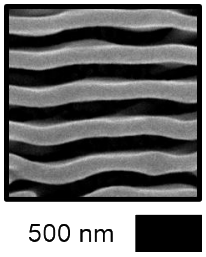


**Figure S6.** Representative top-down SEM of a photoelectrodeposit generated using horizontally polarized $\lambda_{avg}$ = 626 nm illumination.

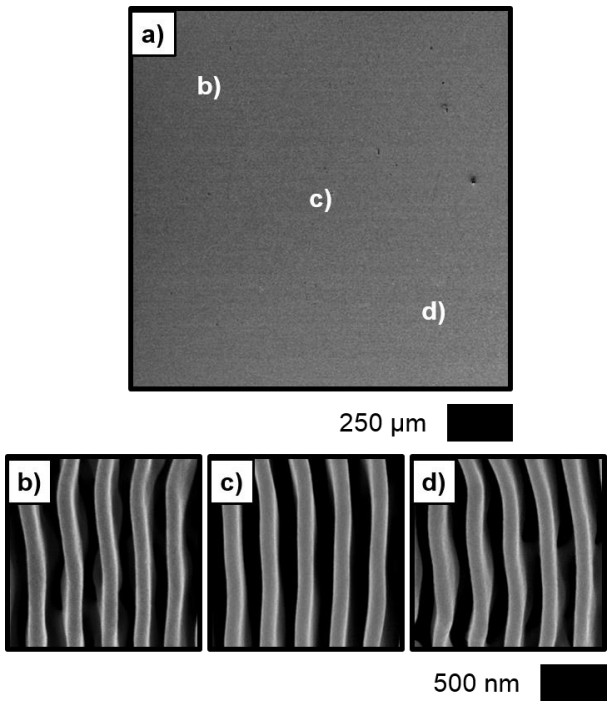


**Figure S7.** (a) Low-magnification SEM of photoelectrodeposit generated using $\lambda_{avg}$ = 626 nm illumination. (b)-(d) High-magnification SEMs acquired from the areas indicated in the SEM presented in (a).

## S6. Additional Computer Simulation Data

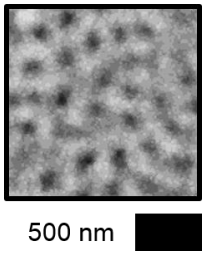


**Figure S8.** Simulated photoelectrodeposit morphology generated using unpolarized $\lambda_{avg}$ = 626 nm illumination.

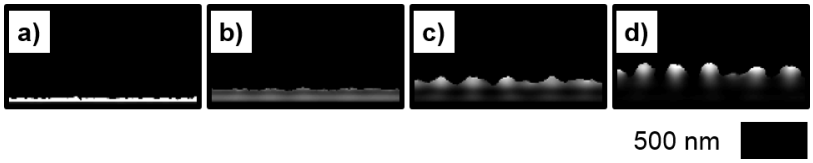


**Figure S9.** (a)-(d) Simulated cross-sectional light absorption profiles for successive stages of photoelectrodeposition using polarized $\lambda_{avg}$ = 626 nm illumination.

Figure S9 presents simulated cross-sectional light absorption profiles, generated using the iterative growth model, for successive stages of photoelectrodeposition using polarized $\lambda_{avg}$ = 626 nm illumination. Initially, the profile is relatively conformal across the surface as the incident illumination is not structured. However, roughness develops due to the random nucleation of the electrodeposited material and effects scattering of the incident illumination leading to non-uniform absorption. Locally elevated light absorption drives locally accelerated rates of material deposition. The evolving surface continues to scatter incident illumination, and interference of the scattered light results in a spatially oscillating absorbance. A periodic lamellar structure emerges wherein absorption is concentrated in the tip of the structure resulting in sustained anisotropic growth.

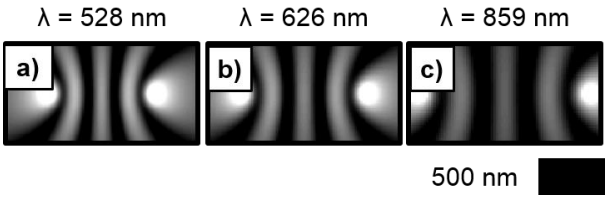


**Figure S10.** (a)-(c) Simulations of normalized time-average electric field magnitudes from two dipoles emitting radiation with indicated free space wavelengths in a medium of index $n$ = 1.33 and separated by a distance of two wavelengths perpendicular to the oscillation axis.

Point dipole sources were used to model the amplitude of the electric field modulation at the nascent growth interface caused by scattering of the incident illumination by the roughness effected by random nucleation of electrodeposited material. Figure S10 presents FDTD simulations of normalized time-averaged electric field magnitudes from two dipoles emitting radiation with free space wavelengths of $\lambda$ = 528 nm (a), 626 nm (b), and 859 nm (c), in a medium of index $n$ = 1.33 and separated by a distance of two wavelengths perpendicular to the oscillation axis. In each case, interference fringes are observed. The spacing and width of the fringes were proportional to the wavelength. This cumulative data is consistent with the observation of increasing lamellar periods and features sizes with increasing values of $\lambda_{avg}$.

The modeling of the initial light scattering at the growth interface using dipole sources (Figure S10), along with the simulated light absorption profiles for successive stages of the photoelectrodeposition process generated using the iterative growth model (Figure S9), together indicate that the fundamental light-matter interactions that optically direct the growth process are principally constrained to the interplay between the deposited material and the incident illumination and independent of the underlying substrate. The light scattering simulations suggest that a spatially oscillating light intensity pattern can be generated from scattering off of electrodeposit nuclei and the light absorption profiles indicate that the incident illumination is strongly absorbed and attenuated by the tips of the deposited structure.

## S7. Additional Grazing Incidence X-Ray Diffraction Data

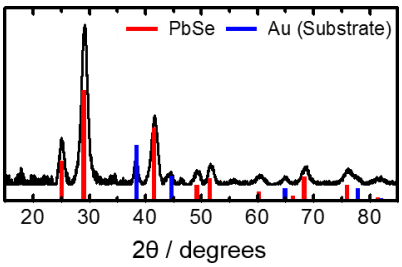


**Figure S11.** GIXRD pattern of a photoelectrodeposit generated with vertically polarized $\lambda_{avg}$ = 626 nm illumination.

Figure S11 presents a GIXRD pattern acquired from a photoelectrodeposit generated with vertically polarized $\lambda_{avg}$ = 626 nm illumination and shows reflections corresponding to polycrystalline PbSe.

## S8. References


1. Humphrey, J. N.; Petritz, R. L. *Phys. Rev.* **1957**, *105*, 1736-1740.

2. El-Korashy, A.; El-Zahed, H.; Zayed, H. A.; Kenawy, M. A. *Solid State Commun.* **1995**, *95*, 335-339.

3. Mott, N. F.; Davis, E. A., *Electronic Processes in Non-Crystalline Materials*. 2 ed.; Oxford University Press: New York, 1971.

4. Tabak, M. D.; Hillegas, W. J. *J. Vac. Sci. Technol.* **1972**, *9*, 387-390.

5. Hale, G. M.; Querry, M. R. *Appl. Opt.* **1973**, *12*, 555-563.